Three Electronic State Model of the Primary Phototransformation of Bacteriorhodopsin*

W. Humphrey[1,2], H. Lu[1,3], I. Logunov[1,4], H.-J. Werner[5] and K. Schulten[1,2,†]

[1]Beckman Institute and Departments of Physics[2], Nuclear Engineering[3], and Chemistry[4], University of Illinois at Urbana-Champaign, Urbana, Illinois 61801

[5]Institut fur Theoretische Chemie, University of Stuttgart, Pfaffenwaldring 55, 70569 Stuttgart, Germany

Classification: Biophysics

October 1, 1996

---

* Abbreviations used: bR, bacteriorhodopsin; DME, density matrix evolution; MD, molecular dynamics.

† To whom correspondence should be addressed. Email: `kschulte@ks.uiuc.edu`

Abstract

The primary all-*trans* $\rightarrow$ 13-*cis* photoisomerization of retinal in bacteriorhodopsin has been investigated by means of quantum chemical and combined classical/quantum mechanical simulations employing the density matrix evolution method. *Ab initio* calculations on an analogue of a protonated Schiff base of retinal *in vacuo* reveal two closely lying excited states S_1 and S_2, the potential surfaces of which intersect along the reaction coordinate through an avoided crossing, and then exhibit a second weakly avoided crossing or a conical intersection with the ground state surface. The dynamics governed by the three potential surfaces, scaled to match the *in situ* level spacings, are described by a combined classical/quantum mechanical simulation in the average state picture. For a suitable choice of non-adiabatic coupling constants the simulations reproduce the observed photoisomerization quantum yield and predict the $S_1 \rightarrow S_2$ crossing at $\tau_1 = 330$ fs and the $S_2 \rightarrow$ ground state crossing at 460 fs after light absorption. The first crossing follows after a 30° torsion on a flat S_1 surface, while the second crossing follows after a rapid torsion by a further 60°. τ_1 matches well the the observed fluorescence life time of S_1. The three level scenario is corroborated by simulations of D85N and D212N mutants of bacteriorhodospin for which τ_1 is found to increase by factors eleven and five, respectively, in qualitative agreement with observations.

Introduction

The protein bacteriorhodopsin (bR) resides in the membrane of the bacterium *Halobacterium halobium* and utilizes sunlight to drive a trans-membrane proton pump in the most basic form of photosynthesis known [1]. The 26 kilodalton protein incorporates a retinal chromophore bound to a lysine residue via a protonated Schiff base linkage and absorbs light around 568 nm. Photoexcitation triggers an isomerization of retinal about its $C_{13}{=}C_{14}$ double bond from an initial all-*trans* to a 13-*cis* configuration which is completed within a few ps. The photoreaction induces a vectorial transfer of a proton, leading to release of a proton to the extracellular side and uptake from the cytoplasmic side. The structure, photocycle, and previous molecular dynamics studies of bR have been reviewed in [2, 3, 4].

The bR photocycle proceeds through several sequential intermediates characterized by distinct retinal absorption maxima. The current view of the photoisomerization process, which has emerged from time-resolved spectroscopy and modeling of the bR photointermediates [5, 6, 7, 8, 9], suggests that the reaction proceeds in the sequential steps

$$\mathrm{bR}_{568} \overset{h\nu}{\rightsquigarrow} \mathrm{bR}^*(200\ \mathrm{fs}) \overset{500\ \mathrm{fs}}{\longrightarrow} \mathrm{J}_{625} \overset{3\ \mathrm{ps}}{\longrightarrow} \mathrm{K}_{590}\ \cdots \tag{1}$$

where photoexcitation of bR generates bR* which successively decays to the intermediates J_{625} and K_{590}, the latter being a ground state product with retinal in a 13-*cis* geometry. The observations suggest that substantial torsional motion takes place during the ∼200 fs lifetime of the excited state bR*. Figure 1

A schematic structure of bR together with retinal bound as a protonated Schiff base here to Lys-216, water molecules and key amino acid side groups Asp-85, Asp-96, and Asp-212 is shown in Fig. 1. Asp-85 is unprotonated and negatively charged at the beginning of the proton pump cycle; this group has been shown in mutagenesis [10, 11, 12] and FTIR experiments [13] to accept a proton from the Schiff base following photoisomerization. The D85N mutant forms the K_{590} intermediate in (1), but exhibits no proton pumping activity [10, 11, 12]. Similarly, the D212N mutant involving another unprotonated aspartic acid side group near retinal fails to pump protons [10, 12]. Following photoexcitation, the excited state dynamics of these mutants differs markedly from the behavior for native bR. The fluorescence lifetime for D85N (D212N) is 20 (4) times longer than the 500 fs lifetime of native bR [14]. The quantum yields of these mutants, nevertheless, are close to the wild-type value of 0.64 ± 0.04 [15, 16, 17, 18].

Previous simulations of the photoisomerization of bR have employed a single potential surface for the excited state, evaluated by means of QCFF/PI methods [19], or being modelled by a simple periodic function [20, 8]. However, polyenes are known to have two closely lying singlet excited states, one of which, $S_{\rm single}$, in case of pure polyenes, is optically allowed and involves mainly single excitations, the other state, $S_{\rm double}$, being optically forbidden and involving mainly two-electron excitations [21, 22, 23, 24]. In polyenes and unprotonated Schiff bases of retinal, $S_{\rm double}$ is the lowest state in energy, while for protonated Schiff bases $S_{\rm single}$ is the lowest state [25]. Photoexcitation of bR populates mainly $S_{\rm single}$, i.e., the lowest excited singlet state; the higher state $S_{\rm double}$ is responsible for the two-photon absorption reported in [26].

The question arises in how far a torsion around retinal's $C_{13}{=}C_{14}$ bond, during photoisomerization, alters the energy level ordering of $S_{\rm single}$ and $S_{\rm double}$ such that the state $S_{\rm double}$

becomes involved in the photodynamics of retinal. This question must be pursued since omission of the second, i.e., higher energy, excited state S_{double} in such a case could affect the photoreaction. In fact, non-adiabatic torsion around the $C_{13}{=}C_{14}$ double bond promotes the two π-electrons residing in the ethylenic ground state of this bond to a double excitation which argues for an involvement of the state S_{double} in the all-*trans* $\rightarrow$ 13-*cis* reaction. The state S_{double} has been shown, indeed, to decrease in energy upon torsion around the double bond of a retinal analogue [4].

Accordingly, we employ in the present study model potential surfaces involving three electronic states suggested in [4]. This model implies that two level crossings are required to return, after photoexcitation, to the ground state. Level crossing is a quantum mechanical process, and for single crossing events one might apply a probabilisitic interpretation of quantum mechanics to account for such events. However, the energetic proximity of the two excited states and the scenario of two level crossings occuring within a few hundred femtoseconds requires a quantum mechanical description in which a 3×3 density matrix accounts for the occupancy of the three participating electronic states and for possible phase coherence [27, 28].

In the following we introduce first the quantum chemical and combined quantum/classical mechanical simulation methods employed in our study. We present then the simulation results demonstrating the participation of three electronic states in the photodynamics of retinal in wild-type bR, and for the D85N and D212N mutants of bR. From these simulations we compute the quantum yield and excited state lifetimes, and compare the results to the experimentally observed photoisomerization reaction dynamics.

Methods

The potential surfaces governing photoisomerization processes have been evaluated *in vacuo* for the retinal analogue $[CH_2–(CH)_3–(C_2H_3)–(CH)_2–NH–CH_3]^+$, at the CASSCF(8,8)/6-31G *ab initio* level by means of the program MOLPRO [29, 30]. This retinal analogue is known to be the shortest analogue that exhibits proton pump activity upon reconstitution with the apoprotein [31]. The utilized complete active space, CAS(8,8), includes the four HOMO and four LUMO orbitals of the full π-orbital space of the four-double-bond retinal analogue. The choice of this analogue was dictated by the fact that retinal itself, which contains six double bonds, proved too large for a sufficiently extensive calculation. The initial geometry of the retinal analogue was minimized at the Hartree-Fock level using the 6-31G basis set; the isomerization potentials were computed for a gradual torsion in steps of 15° around the C=C double bond adjacent to the Schiff base, keeping all other degrees of freedom constant. Basis set improvements beyond the 6-31G level were found not to significantly affect the energetics of isomerization around the relevant double bond of the retinal analogue.

As argued above, one expects the three lowest electronic states (S_0, S_1, and S_2) to be implicated in retinal's photoisomerization. The associated potential surfaces were computed simultaneously by performing state-averaged calculations, in which molecular orbitals are optimized with respect to the average energy of the S_0, S_1, and S_2 states. In regions of close approach between any two surfaces, additional state-averaged calculations were performed to investigate the nature of the "crossing" between the respective states; in such calculations molecular orbitals were optimized with respect to the average energy of the two particular states of interest (either S_0 and S_1, or S_1 and S_2). Figure 2 here

From the adiabatic surfaces in Fig. 2 we change in our simulations to a presentation in terms of a ϕ-dependent 3×3-Hamiltonian matrix H

$$H(\phi) = \begin{pmatrix} E_1(\phi) & V_{12} & V_{13} \\ V_{12} & E_2(\phi) & V_{23} \\ V_{13} & V_{23} & E_3(\phi) \end{pmatrix} \tag{2}$$

where ϕ represents the torsional angle about the $C_{13}=C_{14}$ double bond (the isomerization reaction coordinate), $E_j(\phi)$ are non-adiabatic potential surfaces, and V_{ij} are the non-adiabatic coupling constants which we choose to be ϕ-independent. As discussed further below, the non-adiabatic surfaces E_j and coupling constants V_{ij} were chosen such that the diagonalized form of $H(\phi)$ in Eq. (2) approximates the *ab initio* surfaces of the states S_0, S_1 and S_2 in Fig. 2. In the new representation the regions of non-adiabatic interaction between the states S_0, S_1 and S_2 are represented by explicit crossing points along the $E_j(\phi)$ surfaces.

The use of a truncated retinal analogue and the neglect of the stabilizing effect of the protein environment resulted in an overestimate of the $S_0 \rightarrow S_1$ excitation energy. This deficiency was corrected through a linear scaling of E_1, E_2, and E_3 such that the energy difference between the states S_0 and S_1 at the all-*trans* position measured 50 kcal/mol, a value equal to the excitation energy of retinal in bR. The resulting non-adiabatic surfaces $E_j(\phi)$ are shown in Fig. 3.

The minimum energy separation between S_0 and S_1, as well as between S_1 and S_2, allows one to determine the coupling constants V_{ij}, i.e., the coupling constants should be half of the minimum energy splitting. Instead of adopting such values we employed coupling constants V_{12}, V_{13}, and V_{23} of 0.5, 1, and 1 kcal/mol, respectively, which are considerably smaller than the estimates due to level splittings. However, the latter splittings depend sensitively on the type of state averaging adopted, as discussed further below; certain procedures lead to very small splittings. The value of 0.5 kcal/mol for V_{12} was chosen to enforce agreement with the observed quantum yield of 0.64 [15, 16]; a choice of 1 kcal/mol would result instead in a quantum yield of 0.34. The value of 1 kcal/mol for V_{13} and V_{23} was selected to obtain agreement with the measured lifetime of wild-type bR of about 300 fs in the state S_1 [32]; a value of 3 kcal/mol would yield a crossing time (lifetime) of about 100 fs. Figure 3 here

Hamiltonians similar to (2) were constructed for the bR mutants D85N and D212N absorbing at 615 nm [10] and at 585 nm [33], respectively. For this purpose the minimum of the E_3 surface at the all-*trans* and at the 13-*cis* position was lowered to match the respective excitation energy. The resulting surfaces $E_{3,\mathrm{bR}}$, $E_{3,\mathrm{D85N}}$ and $E_{3,\mathrm{D212N}}$ are compared in Fig. 3.

The photodynamics simulations used as a starting point the refined bR_{568} structure reported in [34] which is based on a structure of bR obtained by electron microscopy [35]. The refined structure includes the loop regions between the seven trans-membrane helices of bR, as well as sixteen water molecules within the protein interior. Five of these water molecules are located within the vicinity of retinal's binding site, in hydrogen-bond contact with the Schiff base proton and nearby amino acids including Asp-85 and Asp-212. D85N and D212N mutants were constructed through modification and equilibration of the refined structure. A series of simulations was carried out for each mutant, each run consisting of a brief 100 fs equilibration starting from a random velocity distribution and using a 1 fs integration time step, followed by simulation of the photoisomerization reaction employing the co-called density matrix evolution (DME) method [36] based on the potential energy surfaces in Fig. 3. The photoisomerization simulations lasted retinal returned to the ground state, and varied from 1 to 12 ps. All simulations which completed a all-*trans* $\rightarrow$ 13-*cis* isomerization were continued for a further 2 ps to model the $J_{625} \rightarrow K_{590}$ transformation; for this purpose the ground state potential introduced in [8] was used to describe the $C_{13}{=}C_{14}$ torsion.

The DME description of the torsion around the $C_{13}{=}C_{14}$ bond couples the evolution of the quantum mechanical density matrix of the three electronic states involved in the photoisomerization with the classical equations of motion of the entire protein [36]. Using the three-state Hamiltonian H in Eq. (2), we introduced the density matrix $\rho(t)$, the diagonal elements of which represent the occupation of the three states as a function of time. Photoexcitation was accounted for by starting from the pure state

$$\rho_{ij}(t_0) = \delta_{33}. \tag{3}$$

During the subsequent simulation, the density matrix evolved according to the Liouville – von Neumann equation

$$\dot{\rho} = \frac{i}{\hbar}\left[\rho, H\right]. \tag{4}$$

The density matrix incorporates the effect of coherence between the quantum states during the dynamics, without the need to calculate the retinal wavefunctions.

The energy stored in the torsion around the $C_{13}{=}C_{14}$ bond is

$$E_{13-14} \;=\; \mathrm{Tr}\,\rho\,H \;=\; \sum_{j=1}^{3} \rho_{jj} E_j \;+\; \sum_{\substack{j,k=1 \\ j\neq k}}^{3} \rho_{jk} V_{kj}\ . \tag{5}$$

The corresponding forces are obtained after taking the (negative) gradient with respect to atomic cordinates. Since the couplings V_{jk} are chosen to be independent of ϕ, the forces acting on atom k with position $\vec{r}_k$ are

$$\vec{F}_{13-14,k}(\phi) \ = \ \sum_{j=1}^{3} \rho_{jj} \vec{F}_{jk} \tag{6}$$

where $\vec{F}_{jk} = -\partial E_j(\phi)/\partial \vec{r}_k$, i.e., the net force acting on an atom is the average over the forces due to each state, weighted by the occupancy ρ_{jj} of that state. To the resulting force on the atom k are added all other forces acting on the atom from the surrounding protein environment.

Equation (4) was integrated by means of a fourth-order Runge-Kutta scheme to yield $\rho(t)$; rapid oscillations in the occupancy of the states required a 0.1 fs integration time step. For the classical molecular dynamics simulations a modified version of the program NAMD [37] was used and a 1 fs integration time step employed. The simulations were carried out at a temperature of 300 K. For the force field, except for the $C_{13}{=}C_{14}$ bond torsion, the CHARMm force field [38] was used, modified for retinal as described previously [8].

Results

The singlet state potential surfaces for torsion around the double bond adjacent to the C=N bond of the retinal analogue $[CH_2–(CH)_3–(C_2H_3)–(CH)_2–NH–CH_3]^+$ are presented in Fig. 2. For the all-*trans* [13-*cis*] geometry the calculations predict, besides the ground state S_0(*trans*) [S_0(13-*cis*)], two closely spaced excited states, a state S_1(*trans*) [S_1(13-*cis*)] with predominantly single-excited electron configurations below a state S_2(*trans*) [S_2(13-*cis*)] with predominantly double-excited electron configurations. This level ordering is in agreement with the configuration interaction calculations on a related polyenylic ion reported in [25]. Due to the lack of symmetry, both $S_1(\textit{trans})$ and $S_2(\textit{trans})$ are optically allowed from the ground state $S_0(\textit{trans})$; the respective transition dipole moments are $\mathrm{D}_{0\to1} = 3.5$ a.u., $\mathrm{D}_{0\to2} = 1.4$ a.u., and $\mathrm{D}_{1\to2} = 1.1$ a.u.

As can be seen from Fig. 2, the potential surfaces along the complete [0°, 180°] interval of the torsional angle ϕ exhibit three avoided crossings, two near $\phi_1 = 30°$, $\phi_1' = 150°$, and one near $\phi_2 = 90°$. Following the procedure outlined in Methods, the surfaces can be interpreted as arising from three adiabatic surfaces shown in Fig. 3, one surface (E_2) connecting the all-*trans* ground state $S_0(\textit{trans})$ to the excited state S_2(13-*cis*), a second (E_1) connecting conversely the excited state $S_2(\textit{trans})$ to the ground state S_0(13-*cis*), and a third one ($E_{3,\mathrm{bR}}$) connecting the excited state $S_1(\textit{trans})$ to the excited state S_1(13-*cis*).

The identification of the two adiabatic surfaces E_1 and E_2 constitutes a key result of this paper on which the further description is based. The surface E_2 is consistent with the simple interpretation that the state $\mathrm{S}_0(\textit{trans})$ contains two π-electrons in the bonding orbital of the double bond under consideration, and that a 180° torsion adabatically lifts these π-electrons into the anti-bonding orbital, i.e., into a doubly excited electron configuration; the occurence of such configurations is characteristic of the S_2(13-*cis*) state. The surface E_1 can be interpreted in a similar manner.

The distinctive feature of the surfaces in Figs. 2, 3 is the existence of regions of non-adiabatic interactions inducing, near ϕ_1 (ϕ_1'), the crossing $E_1 \leftrightarrow E_{3,\mathrm{bR}}$ ($E_2 \leftrightarrow E_{3,\mathrm{bR}}$) and, near ϕ_2, the crossing $E_1 \leftrightarrow E_2$. We examined the surfaces near ϕ_1 by means of the quantum chemical calculations outlined above state averaging over the S_1 and S_2 states, i.e., involving only the two states participating in the crossing $E_{3,\mathrm{bR}} \leftrightarrow E_1$. The results revealed that the interaction in this region is of the "avoided crossing" type; the potential curves obtained in state-average calculations for the two states do not differ considerably from those presented in Fig. 2, implying that the coupling between the S_1 and S_2 states in the ϕ_1 region is strong.

In contrast, examination of the potential surface in the region near ϕ_2, employing averaging over only the two states S_0 and S_1, leads to results which differ considerably from those obtained when all three states are involved in the average. This is demonstrated in the inset in Fig. 2, which shows that the separation between the surfaces becomes less than 1 kcal/mole in this case. Most likely, the crossing between S_0 and S_1 is of the "conical intersection" type [39]. Clarification of this matter requires consideration of further retinal degrees of freedom in the crossing region, e.g., of the stretch vibration of the $C_{13}{=}C_{14}$ bond [39]. Calculations performed for a smaller retinal analogue indicate, indeed, the existence of a conical intersection between S_0 and S_1 [40].

The features outlined suggest that a sufficiently strong non-adiabatic coupling between the $E_{3,\mathrm{bR}}$ and E_1 surfaces near ϕ_1 is required for the photoisomerization process to induce the necessary transition $E_{3,\mathrm{bR}} \rightarrow E_1$, while weak interaction between the E_1 and the E_2 surfaces are preferable, since the latter favors continuation of the torsion on the E_1 surface (see Fig. 3) towards the 13-*cis* geometry. Figure 4

As outlined in Methods, the non-adiabatic potential surfaces in Fig. 3 served to carry out a combined quantum/classical mechanical simulation, resulting in trajectories which provide coordinates, e.g., the torsional angle of the $C_{13}{=}C_{14}$ bond $\phi(t)$, as well as selected observables, e.g., the energy E_{13-14} define in Eq. (5). Figure 4 presents the $[E_{13-14}(t), \phi(t)]$ diagram of a typical trajectory resulting from a 1 ps simulation. Retinal is excited initially here in the all-*trans* geometry by a 568 nm photon, i.e., placed on the $E_{3,\mathrm{bR}}$ surface at $\phi = 0$ [c.f., Eq. (3)]; after a time τ_1 the system crosses to the surface E_1, where it quickly descends to the second crossing point ϕ_2 at time τ_2. Here, after a brief period of meandering near the crossing point, the system chooses to continue along E_1 to complete the photoisomerization and reaches the 13-*cis* geometry. The energy $E_{13-14}(t)$, initially, follows closely the potential surfaces, but at the end of the photoreaction deviates significantly from the surface $E_1[\phi(t)]$, reflecting the fact that the system is trapped in a mixed quantum state.

The character of the quantum state is characterized by the diagonal elements ρ_{jj}, $j = 1, 2, 3$ of the density matrix, which describe the occupancies of the three electronic states corresponding to the surfaces E_1, E_2, $E_{3,\mathrm{bR}}$. These occupancies are shown in Fig. 5. Following excitation, i.e., at $t_0 = 0$, the occupancies of states corresponding to E_1 and $E_{3,\mathrm{bR}}$ oscillate rapidly for about 200 fs due to the energetic proximity of the surfaces. The system is then seen to switch rapidly to the surface E_1, whereupon a fast torsion moves the system in a time $\Delta\tau$ (see Table 1) to the second crossing point with the surface E_2. Rapid oscillations are again discernible at this stage, mixing the states corresponding to E_1 and E_2; due to the rather weak non-adiabatic coupling $V_{12} = 0.5$ kcal/mol, the system chooses to stay on the E_1 surface. However, beyond the crossing point the states corresponding to E_2, $E_{3,\mathrm{bR}}$ remain populated to a significant degree. Due to environmental relaxation effects, not accounted for in our description, the occupancies of these states should vanish within about ten femtoseconds as demonstrated recently for a hydrated electron for which relaxation effects are expected to be stronger, however, than in the present case [41]. The neglect of this decay is a shortcoming of the approach adopted here which, as a result, can lead to unphysical "average" final states, when in reality the system would choose between one of many possible outcomes with some probability distribution. Figure 5 here

In all our simulations of the photoisomerization event in bR and its mutants, the final product exhibited over 50% occupancy of either of the states corresponding to E_1 or E_2; in the example shown in Figs. 4, 5, the occupancy is almost 90%. After completion of the photoisomerization, our simulations switched from the DME approach to the torsional potential as used in conventional simulations.

An alternate scheme which has been employed in combined quantum/classical molecular dynamics simulations is the surface-hopping algorithm [42, 43]. In this scheme, the system is taken to occupy only one state at any given time; after each integration time step, the system may switch from the current state to another state with a probability designed to minimize the number of transitions while providing the correct statistical occupation of each state. A benefit of this method is that it will generate proper asymptotic behavior since the system cannot occupy an average state. The probabilistic nature of the method, however, requires in many cases a large number of iterations for proper convergence. Thus, application of the surface-hopping algorithm in this study was not feasible due to the extensive computational requirements.

A total of 100 simulations of the photoisomerization of wild-type bR were carried out resulting in trajectories like the one shown in Figs. 4, 5. Fifty simulations were also completed for the D85N and D212N mutants of bR, by replacing the potential surface $E_{3,\mathrm{bR}}$ by the surfaces $E_{3,\mathrm{D85N}}$ and $E_{3,\mathrm{D212N}}$ shown in Fig. 3. The simulations for the mutants required simulation periods of 1–12 ps due to the longer time required for retinal in D85N and

D212N bR to cross to the E_1 potential surface. The results of the simulations are presented in Table 1. For each set of simulations, the fraction of trials which completed the all-*trans* $\rightarrow$ 13-*cis* isomerization were identified and the average crossing times τ_1 and τ_2 were determined. Table 1

In the 100 simulations of wild-type bR, 71 13-*cis* products emerged. Trials which failed here
to form a 13-*cis* isomer either did not move beyond the first crossing point ϕ_1 or switched to the surface E_2 at the second crossing point ϕ_2, i.e., such trials reformed all-*trans* retinal. The simulated photoisomerization quantum yield measured 0.71 for wild-type bR, matching closely the observed quantum yield of 0.64 $\pm$ 0.04 [15, 16]. The agreement, however, is a consequence of the choice of coupling between the E_1 and E_2 surfaces as stated in Methods.

Time-resolved spectroscopy of bR has revealed two fast processes, one occuring within 200 $\pm$ 70 fs [6], and the other occuring within 500 $\pm$ 100 fs [5, 6, 7]. The observations were interpreted to suggest that photoexcitation is followed by rapid progression along the reaction coordinate from all-*trans* to 13-*cis* during the initial 200 fs. More recently, however, femtosecond spectroscopy covering an extremely wide spectral range has indicated a lack of a spectral shift of induced absorption, indicating a flat excited state surface; the observations revealed also a relaxation processes with a decay time of 370 fs [32]. The $E_{3,\mathrm{bR}} \rightarrow E_1$ crossing at $\tau_1 = 332$ fs can explain the observed fast decay.

Figures 4, 5 show the behavior of a single, albeit typical, quantum/classical mechanical trajectory. Of interest is the average behavior of bR. The inset in Fig. 5 shows the time evolution of the density of the states corresponding to the surfaces E_1, E_2 and $E_{3,\mathrm{bR}}$ averaged over all 71 simulations which formed 13-*cis* photoproducts. The time at which the occupation of $E_{3,\mathrm{bR}}$ and E_1 intersect is τ_1, while τ_2 is near the time where the occupation of E_1 exceeds 50%. One can discern that retinal photoisomerizes within about 500 fs to the 13-*cis* geometry with a final populaton of the E_1 surface, on average, of about 80%.

For the D85N and D212N mutants of bR the dynamics of retinal after light excitation is significantly slower in the initial phase. This is due to the fact that the surfaces $E_{3,\mathrm{D8N}}$ and $E_{3,\mathrm{D212N}}$ cross the E_1 surfaces at higher energies than in case of the $E_{3,\mathrm{bR}} \rightarrow E_1$ crossing. As a result, for D85N bR, of which 30 of 50 simulations formed 13-*cis* isomers, the average time to the first crossing point was 5.59 ps. In case of D212N bR with 37 out of 50 completing the 13-*cis* isomerization, the first crossing occurred at 3.24 ps. Interestingly, the time between the first and the second crossing, $\Delta\tau$, measured approximately the same for native bR and for its D85N or D212N mutants; the mutants spent the major part of the reaction time before encountering the first crossing point.

In previous molecular dynamics simulations of the photoisomerization of retinal in bR [8, 4], the isomerization products assumed two distinct structures: case one structures, in which the Schiff base N-H$^+$ bond is oriented towards the cytoplasmic side of the protein, and case two structure, in which twists around retinal's single bonds oriented the N-H$^+$ bond to point parallel to the plane of the membrane and to remain connected to Asp-85 via hydrogen-bonds with an intermediate water molecule. The latter product was identified with the K_{590} intermediate which actually initiates the proton pump cycle [8, 4, 44]. Figure 6 compares the retinal binding site region for a case one (Fig. 6b) and case two (Fig. 6c) with the all-*trans* retinal binding site (Fig. 6a). The combined quantum/classical simulation of the present study led 66% case one products and 34% case two products formed. This distribution is similar to that in the earlier simulations (58% and 36%, respectively). The present work supports, therefore, the conclusions reached previously regarding a possible mechanism of bR's pump cycle [4, 44]. Figure 6 here

Discussion

The excited state dynamics of retinal in bR, starting from light absorption into the first excited state, proceeds rapidly as a torsion around the $C_{13}{=}C_{14}$ bond and is characterized by two crossing events: one crossing involves relatively strong non-adiabatic coupling between the first and second excited states at a nearly 30° torsion 332 fs after light absorption; a second crossing occurs between the second excited state and the ground state, in which retinal moves essentially along a steep non-adiabatic surface, completing a 60° motion in another 130 fs. A choice of non-adiabatic couplings of the order of 1 kcal/mol can explain the overall quantum yield. Due to interaction with the protein, two isomerized reaction products arise, one with the Schiff base proton in hydrogen bond contact with Asp-85, the other with the Schiff base proton pointing to Asp-96 on the cytoplasmic side.

First Crossing Following photoexcitation from the ground state surface E_1 to the excited state surface $E_{3,\mathrm{bR}}$, retinal rotates around its $C_{13}{=}C_{14}$ bond until it reaches the first crossing point ϕ_1. In this region, interaction with the nearly degenerate excited state E_2 allows the system to overcome the slight energy barrier before crossing to E_1. For the wild-type, this crossing point was reached after 332 fs, which compares quite well with time-resolved spectroscopy measurements of this process by Hasson and coworkers if one associates the observed 370 fs fast relaxation process [32] with the crossing event. The near degeneracy of the surfaces $E_1(\phi)$ and $E_{3,\mathrm{bR}}(\phi)$ for small angles ϕ implies a continuous interaction which prepares retinal for the crossing and induces it for a relatively small non-adiabatic coupling; thus, the interaction of the system in the region of the first crossing region does not affect the quantum yield. In almost all simulations, retinal eventually surmounted the slight all-*trans* $\rightarrow \phi_1$ energy barrier of 1–3 kcal/mol. The important characteristic of the initial phase of the excited state dynamics is that retinal remains very close to its all-*trans* geometry; rapid torsion sets in only after the first crossing is completed.

Second Crossing Upon reaching the second crossing point ϕ_2, near the 90° torsion, retinal makes a non-adiabatic transition to the ground state characterized by very weak coupling between the respective non-adiabatic surfaces. Essentially, retinal moves along the non-adiabatic surface $E_1(\phi)$ (see Fig. 3), halting briefly at the crossing point as shown in Fig. 4. The brief halt at the crossing points makes it unlikely that this stage of the photodynamics can be identified with the J_{625} intermediate. The crossing determines, however, the quantum yield of formation of 13-*cis*-products; the observed value of 0.71 [15, 16] is reproduced only for a weak coupling $V_{12} = 0.5$ kcal/mol. The second crossing point is reached within 462 fs for wild-type bR, while a slower decay process on the order of 1 ps has been observed by Hasson *et al.* [32]. The difference may stem from an asymmetry in the real potential energy surfaces or from an alternative interpretation of the observed relaxation.

Photodynamics of bR Mutants The D85N and D212N mutants of bR exhibit strongly increased fluorescence life times without changes in the quantum yield [14], a behavior which is explained well by the three state model through an increase of the barrier for the first crossing event. The schematic potential surfaces employed in the simulations cannot be expected to reproduce exact crossing times. The close agreement for wild-type bR is due to the choice of the coupling $V_{12} = 1$ kcal/mol. Nevertheless, our results provide a possible explanation of the behavior of bR mutants. Assuming that the crossing times are governed by a Boltzmann distribution at the crossing point ϕ_1 relative to the all-*trans* position, and that the crossing points are at the same absolute height, the ratio of the mutants' excited state lifetimes to that of bR is

$$\frac{\tau_{2,mutant}}{\tau_{2,bR}} \approx \exp\left[\frac{\Delta E_{3,mutant} - \Delta E_{3,bR}}{kT}\right], \tag{7}$$

where $\Delta E_{3,mutant} = E_{3,mutant}(\phi_1) - E_{3,mutant}(trans)$. Accordingly, mutations which shift the retinal absorption to the red increase the barrier to photoisomerization and lead to longer excited state lifetimes. Inserting for $\Delta E_{3,mutant}$ in Eq. (7) the values corresponding to the spectral shifts experienced by the D85N and D212N mutants predicts lifetime increases by factors of 20 and 1.8, respectively, for the mutants.

The quantum yield for mutants such as D85N and D212N has been found experimentally to be similar to the wild-type value [17, 18], and the yield obtained for these mutants in our simulations was likewise similar (0.60 and 0.74 for D85N and D212N, respectively, compared to 0.71 for the wild-type).

Conclusions

In summary, combined quantum/classical simulations of the bR photoisomerization supports a new model of the very early events in the bR photocycle, differing from previous models based on ultrafast spectroscopy [5, 6, 7]. In the new model, photoexcitation of retinal is followed not by rapid movement along the reaction coordinate due to excitation into a repulsive Frank-Condon region, but by motion along a relatively flat excited state surface until crossing to a region with a second excited state, which exhibits a steep potential gradient inducing rapid isomerization. A proper description of this behavior requires inclusion of at least the first two excited states. The observed spectral and fluorescent changes occuring within 1 ps after photoexcitation of bR arise due to non-adiabatic transitions between the excited states and an excited state and the ground state. A significant fraction of the excited state lifetime is spent surmounting a small energy barrier before reaching the first non-adiabatic crossing region. The fluorescence lifetime of bR is controlled by this barrier and can be altered strongly through mutations which affect the relative stability of retinal's two lowest excited states.

Acknowledgements

This work was supported by grants from the National Institutes of Health (PHS 5 P41 RR05969-04), the National Science Foundation (BIR-9318159), and the Roy J. Carver Charitable Trust.

References

(1) Lozier, R. H., Bogomolni, R. A., & Stoeckenius, W. (1975). *Biophys. J.* **15**, 955–962.

(2) Oesterhelt, D., Tittor, J., & Bamberg, E. (1992). *J. Bioenerg. Biomemb.* **24**, 181–191.

(3) Ebrey, T. (1993). In Jacobson, M., editor, *Thermodynamics of Membranes, Receptors and Channels*, pages 353–387. CRC Press, New York.

(4) Schulten, K., Humphrey, W., Logunov, I., Sheves, M., & Xu, D. (1995). *Israel Journal of Chemistry* **35**, 447–464.

(5) Mathies, R. A., Brito Cruz, C. H., Pollard, W. T., & Shank, C. V. (1988). *Science* **240**, 777–779.

(6) Dobler, J., Zinth, W., Kaiser, W., & Oesterhelt, D. (1988). *Chem. Phys. Lett.* **144**, 215–220.

(7) Du, M. & Fleming, G. (1993). *Biol. Cybernetics* **48**, 101–111.

(8) Humphrey, W., Xu, D., Sheves, M., & Schulten, K. (1995). *J. Phys. Chem.* **99**, 14549–14560.

(9) Xu, D., Martin, C., & Schulten, K. (1996). *Biophys. J.* **70**, 453–460.

(10) Mogi, T., Stern, L., Marti, T., Chao, B., & Khorana, H. (1988). *Proc. Natl. Acad. Sci. USA* **85**, 4148–4152.

(11) Subramaniam, S., Marti, T., & Khorana, H. G. (1990). *Proc. Natl. Acad. Sci. USA* **87**, 1013–1017.

(12) Otto, H., Marti, T., Holz, M., Mogi, T., Stern, L. J., Engel, F., Khorana, H. G., & Heyn, M. P. (1990). *Proc. Natl. Acad. Sci. USA* **87**, 1018–1022.

(13) Braiman, M. S., Mogi, T., Marti, T., Stern, L. J., Khorana, H. G., & Rothschild, K. J. (1988). *Biochemistry* **27**, 8516–8520.

(14) Song, L., El-Sayed, M. A., & Lanyi, J. K. (1993). *Science* **261**, 891–894.

(15) Schneider, G., Diller, R., & Stockburger, M. (1989). *Chem. Phys.* **131**, 17–29.

(16) Govindjee, R., Balashov, S. P., & Ebrey, T. G. (1990). *Biophys. J.* **58**, 597–608.

(17) Logunov, S., El-Sayed, M., & Song, L. (1996). *J. Phys. Chem.* **100**, 2391–2398.

(18) Logunov, S., El-Sayed, M., & Lanyi, J. (1996). *Biophys. J.* **70**, 2875–2881.

(19) Warshel, A., Chu, Z. T., & Hwang, J.-K. (1991). *Chem. Phys.* **158**, 303–314.

(20) Zhou, F., Windemuth, A., & Schulten, K. (1993). *Biochemistry* **32**, 2291–2306.

(21) Schulten, K. & Karplus, M. (1972). *Chem. Phys. Lett.* **14**, 305–309.

(22) Hudson, B. S., Kohler, B. E., & Schulten, K. (1982). In Lim, E. C., editor, *Excited States*, volume 6, pages 1–95. Academic Press.

(23) Tavan, P. & Schulten, K. (1986). *J. Chem. Phys.* **85**, 6602–6609.

(24) Serrano-Andreas, L., Lindh, R., Roos, B., & Merchan, M. (1993). *J. Phys. Chem.* **97**, 9360–9368.

(25) Schulten, K., Dinur, U., & Honig, B. (1980). *J. Chem. Phys.* **73**, 3927–3935.

(26) Birge, R. R. & Zhang, C. F. (1990). *J. Chem. Phys.* **92**, 7178–7195.

(27) Mavri, J., Berendsen, H. J. C., & Gunsteren, W. F. V. (1993). *J. Phys. Chem.* **97**, 13469–13476.

(28) Schulten, K. (1995). In Bicout, D. & Field, M. J., editors, *Proceedings of the Ecole de Physique des Houches*, pages 85–118, Paris. Les Editions de Physique, Springer.

(29) Werner, H.-J. & Knowles, P. J. (1985). *J. Chem. Phys.* **82**, 5053–5063.

(30) Knowles, P. J. & Werner, H.-J. (1985). *Chem. Phys. Lett.* **115**, 259–267.

(31) Steinberg, G., Friedman, N., Sheves, M., & Ottolenghi, M. (1991). *Photochem. Photobiol.* **54**, 969–676.

(32) Hasson, K., Gai, F., & Anfinrud, P. (1996). *Proc. Natl. Acad. Sci. USA*. Submitted.

(33) Needleman, R., Chang, M., Ni, B., Varo, G., Fornes, J., White, S. H., & Lanyi, J. K. (1991). *J. Biol. Chem.* **266**, 11478–11484.

(34) Humphrey, W., Logunov, I., Schulten, K., & Sheves, M. (1994). *Biochemistry* **33**, 3668–3678.

(35) Henderson, R., Baldwin, J. M., Ceska, T. A., Zemlin, F., Beckmann, E., & Downing, K. H. (1990). *J. Mol. Biol.* **213**, 899–929.

(36) Berendsen, H. & Mavri, J. (1993). *J. Phys. Chem.* **97**, 13464–13468.

(37) Nelson, M., Humphrey, W., Gursoy, A., Dalke, A., Kalé, L., Skeel, R., Schulten, K., & Kufrin, R. (1995). *Comput. Phys. Commun.* **91**, 111–134.

(38) Brooks, B. R., Bruccoleri, R. E., Olafson, B. D., States, D. J., Swaminathan, S., & Karplus, M. (1983). *J. Comp. Chem.* **4**, 187–217.

(39) Cederbaum, L. S., Köppel, H., & Domcke, W. (1981). *Int. J. Quantum Chem. Symp.* **15**, 251–267.

(40) Bonacic-Koutecky, V., Schoffel, K., & Michl, J. (1987). *Theoret. Chim. Acta* **72**, 459–474.

(41) Schwartz, B., Bittner, E., Prezhdo, O., & Rossky, P. (1996). *J. Chem. Phys.* **104**, 5492–5955.

(42) Tully, J. C. & Preston, R. (1971). *J. Chem. Phys.* **55**, 562.

(43) Tully, J. C. (1990). *J. Chem. Phys.* **93**, 1061–1071.

(44) Xu, D., Sheves, M., & Schulten, K. (1995). *Biophys. J.* **69**, 2745–2760.

Figure Captions

Table 1: Summary of photodynamics simulation results. ϕ_1 and ϕ_2 are torsional angles of the C_{13}=C_{14} bond at the first and second crossing points; τ_1 and τ_2 are the average times required to reach these points. $\Delta\tau$ is the difference between τ_2 and τ_1. λ_{max} values are from [10, 33].

Figure 1: The protein bacteriorhodopsin, including retinal, water molecules, and residues Asp-85, Asp-96, Asp-212, Arg-82, and Glu-204 which participate in proton translocation. Portions of helices C and D have been removed to reveal the protein interior.

Figure 2: Computed ground and excited state potentials of [H_2C=(CH)–(CH)=(CH)–(CH_2-C^*)=(C^*H)–(CH)=NH^+–CH_3], an analogue of the protonated Schiff base of retinal. The dependence of the energies of the ground state (S_0) as well as the first (S_1) and second (S_2) excited states on the torsional angle ϕ of the bond C^*=C^* is shown. The bond C^*=C^* corresponds to the C_{13}=C_{14} double bond of retinal. State-average calculations for the S_0, S_1, and S_2 electronic states were performed at the CASSCF(8,8)/6-31G *ab initio* level (see text). ϕ_1 and ϕ_2 indicate the two regions of close interaction between the two excited states, and between the first excited state and the ground state, respectively.

Figure 3: Non-adiabatic potential energy surfaces used in molecular dynamics simulations of bacteriorhodopsin and bR mutants. The minimum of the surfaces $E_{3,\mathrm{bR}}$, $E_{3,\mathrm{D85N}}$, and $E_{3,\mathrm{D212N}}$ are matched to the measured excitation energy bR and its respective mutants.

Figure 4: Energy of the C_{13}-C_{14} torsional degree of freedom E_{13-14} as a function of the torsional bond angle ϕ, i.e., $[E_{13-14}(t),\, \phi(t)]$ trajectory, for a sample molecular dynamics simulation, compared to the three non-adiabatic energy surfaces E_1, E_2, and $E_{3,\mathrm{bR}}$ shown in Fig. 3. Initially retinal is promoted in the all-*trans* geometry from E_2 to $E_{3,\mathrm{bR}}$; subsequently, retinal crosses to E_1 near $\phi\ = \phi_1$. At $\phi\ = \phi_2$ retinal may choose to continue its motion along E_1 to reach the 13-*cis* geometry as shown, or it may cross to E_2 to reform the all-*trans* state (not shown).

Figure 5: Occupancies $\rho_{jj}(t)$ of the three non-adiabatic potential energy surfaces E_1, E_2, and $E_{3,\mathrm{bR}}$ as a function of time for the $[E_{13-14}(t),\ \phi(t)]$ trajectory shown in Fig. 4. In the inset are shown the occupancies averaged over all simulations which resulted in 13-*cis* retinal.

Figure 6: (a) Retinal and its binding site in bR, including residues Asp-85, Asp-212, and internal water molecules. (b) Case 1 13-*cis* photoproduct. (c) Case 2 13-*cis* photoproduct.

	Bacteriorhodopsin Mutant		
	bR_{568}	D85N	D212N
λ_{max}	568 nm	615 nm	585 nm
Simulations	100	50	50
13-*cis* Products	71	30	37
Case 1 Products	66%	83%	84%
Case 2 Products	34%	0%	5%
ϕ_1	152.2°	144.1°	148.7°
τ_1	332 fs	5.59 ps	3.24 ps
ϕ_2	90°	90°	90°
τ_2	462 fs	5.73 ps	3.42 ps
$\Delta\tau$	130 fs	140 fs	178 fs
$\tau_2\,(\text{mutant})/\tau_2\,(\text{bR})$	-	12.4	7.4

Table 1: Summary of photodynamics simulation results. ϕ_1 and ϕ_2 are torsional angles of the C_{13}=C_{14} bond at the first and second crossing points; τ_1 and τ_2 are the average times required to reach these points. $\Delta\tau$ is the difference between τ_2 and τ_1. λ_{max} values are from [10, 33].

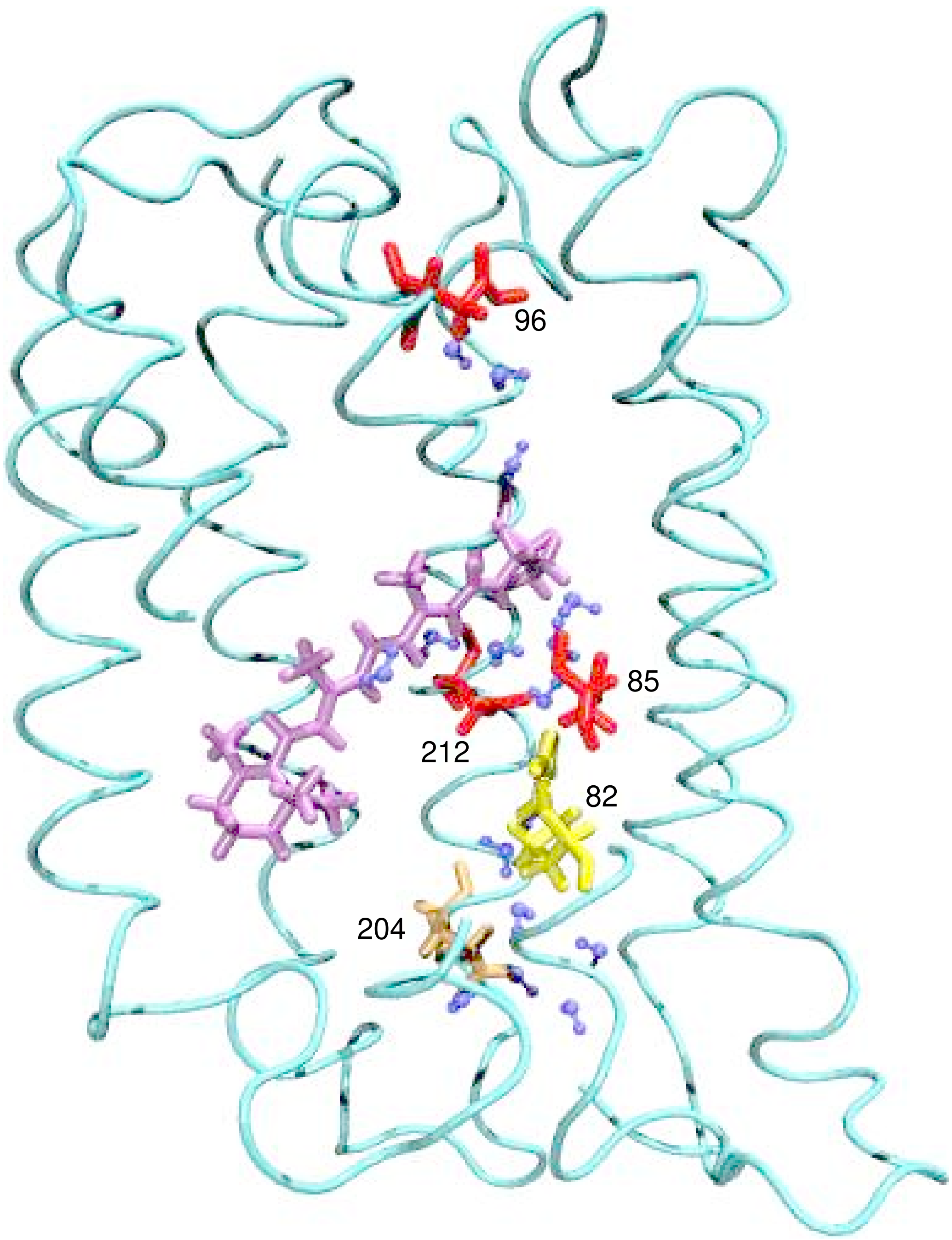

Figure 1: The protein bacteriorhodopsin, including retinal, water molecules, and residues Asp-85, Asp-96, Asp-212, Arg-82, and Glu-204 which participate in proton translocation. Portions of helices C and D have been removed to reveal the protein interior.

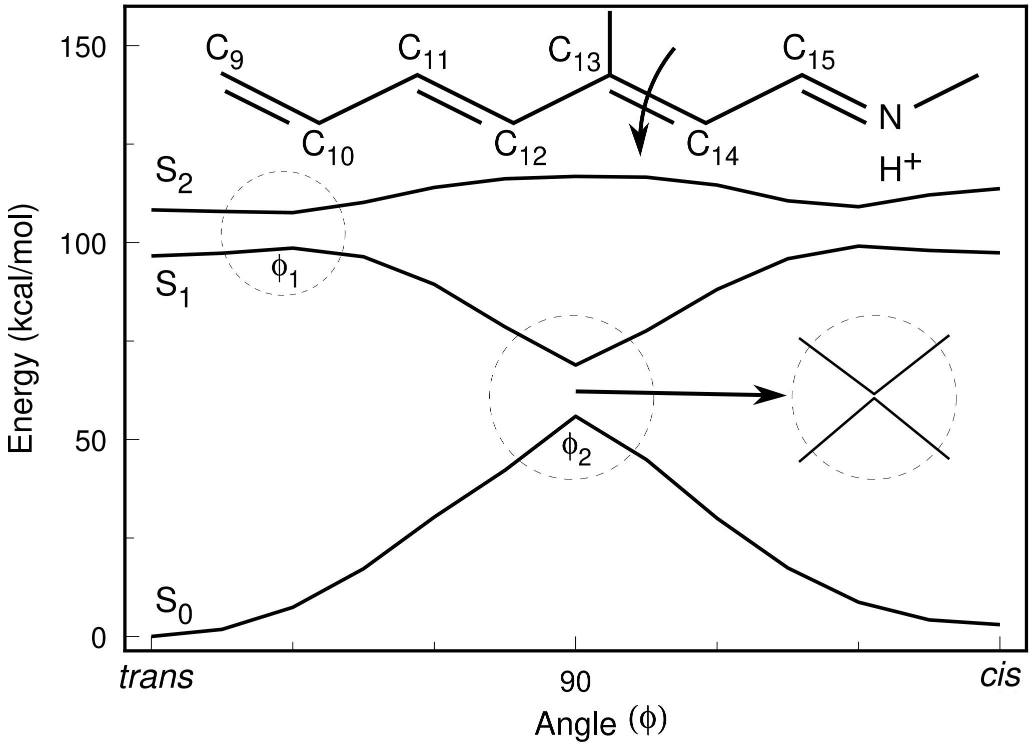

Figure 2: Computed ground and excited state potentials of [H_2C=(CH)–(CH)=(CH)–(CH_2-C^*)=(C^*H)–(CH)=NH^+–CH_3], an analogue of the protonated Schiff base of retinal. The dependence of the energies of the ground state (S_0) as well as the first (S_1) and second (S_2) excited states on the torsional angle ϕ of the bond C^*=C^* is shown. The bond C^*=C^* corresponds to the C_{13}=C_{14} double bond of retinal. State-average calculations for the S_0, S_1, and S_2 electronic states were performed at the CASSCF(8,8)/6-31G *ab initio* level (see text). ϕ_1 and ϕ_2 indicate the two regions of close interaction between the two excited states, and between the first excited state and the ground state, respectively.

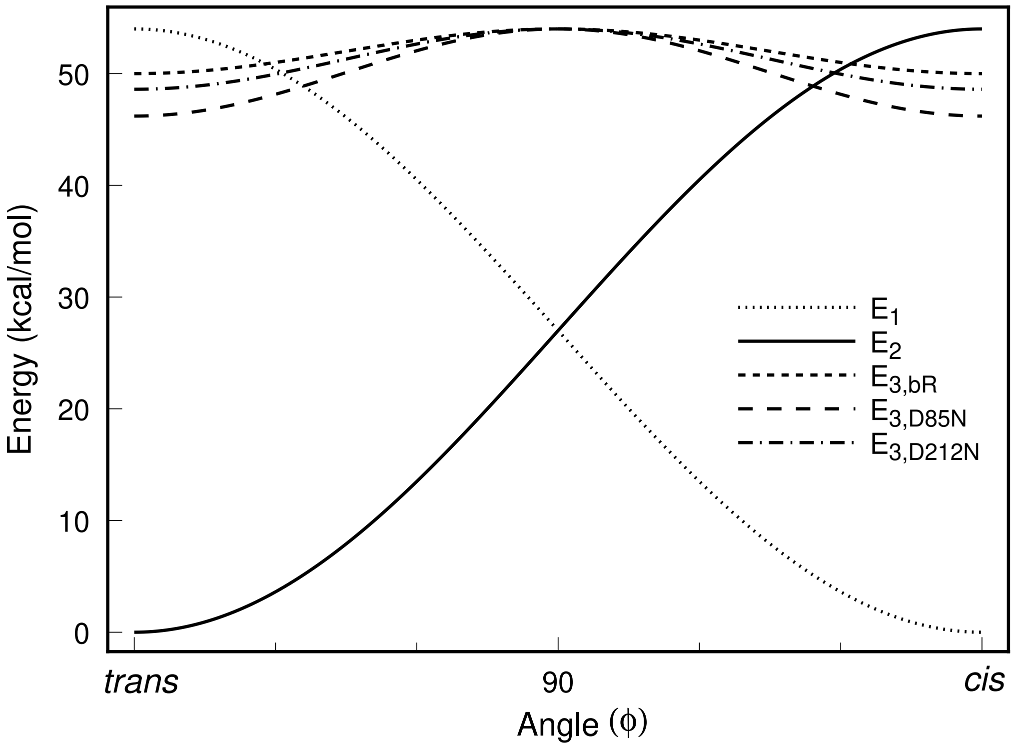

Figure 3: Non-adiabatic potential energy surfaces used in molecular dynamics simulations of bacteriorhodopsin and bR mutants. The minimum of the surfaces $E_{3,\mathrm{bR}}$, $E_{3,\mathrm{D85N}}$, and $E_{3,\mathrm{D212N}}$ are matched to the measured excitation energy bR and its respective mutants.

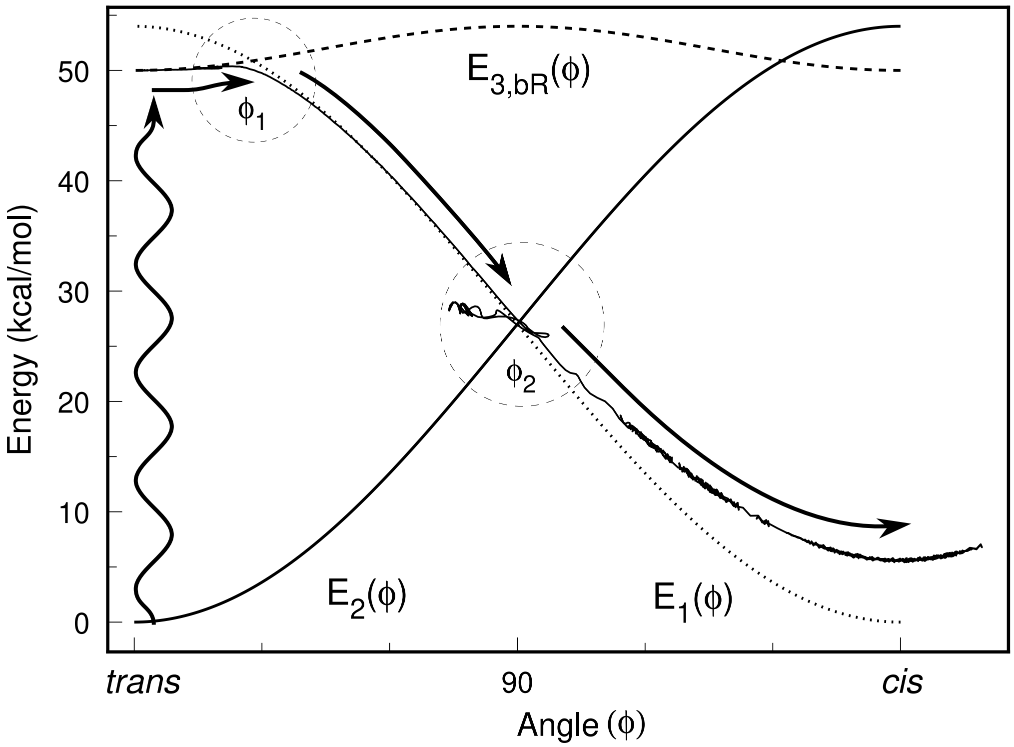

Figure 4: Energy of the C_{13}-C_{14} torsional degree of freedom E_{13-14} as a function of the torsional bond angle ϕ, i.e., $[E_{13-14}(t),\ \phi(t)]$ trajectory, for a sample molecular dynamics simulation, compared to the three non-adiabatic energy surfaces E_1, E_2, and $E_{3,\mathrm{bR}}$ shown in Fig. 3. Initially retinal is promoted in the all-*trans* geometry from E_2 to $E_{3,\mathrm{bR}}$; subsequently, retinal crosses to E_1 near $\phi\ = \phi_1$. At $\phi\ = \phi_2$ retinal may choose to continue its motion along E_1 to reach the 13-*cis* geometry as shown, or it may cross to E_2 to reform the all-*trans* state (not shown).

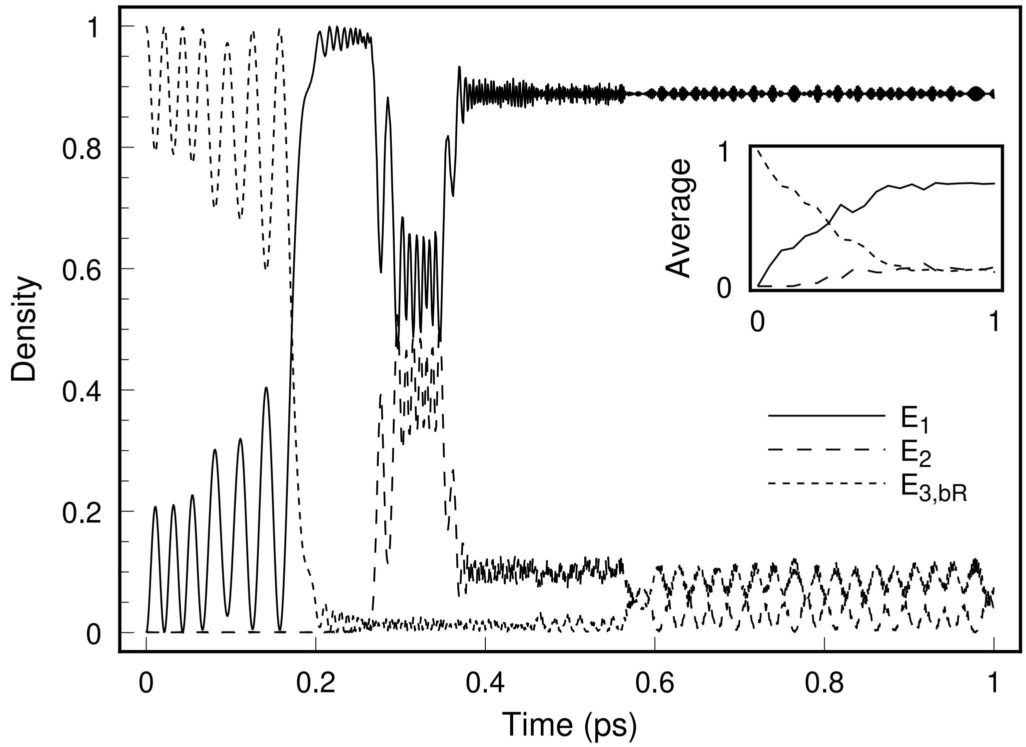

Figure 5: Occupancies $\rho_{jj}(t)$ of the three non-adiabatic potential energy surfaces E_1, E_2, and $E_{3,\mathrm{bR}}$ as a function of time for the $[E_{13-14}(t),\ \phi(t)]$ trajectory shown in Fig. 4. In the inset are shown the occupancies averaged over all simulations which resulted in 13-*cis* retinal.

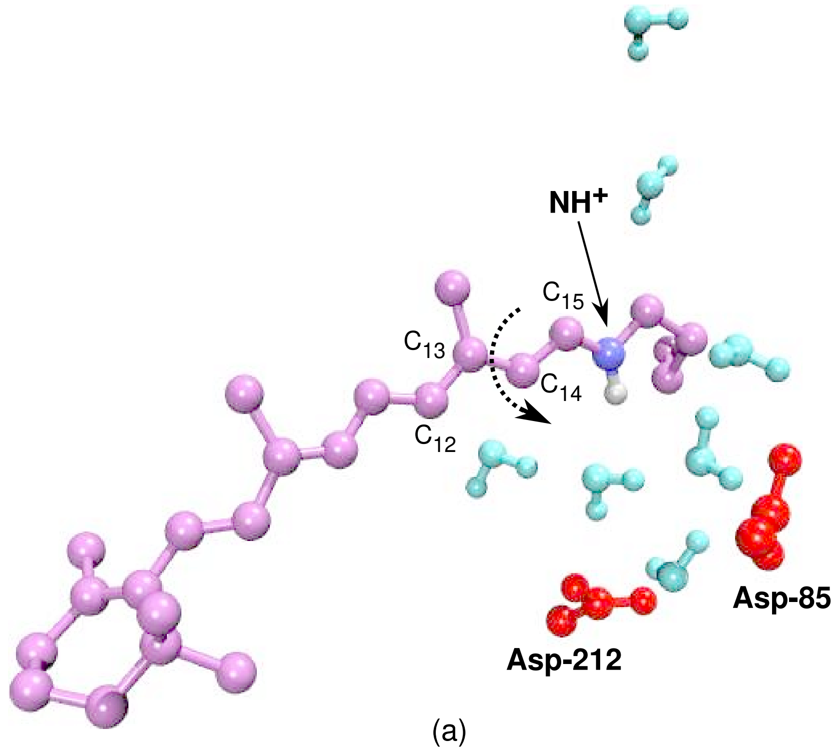

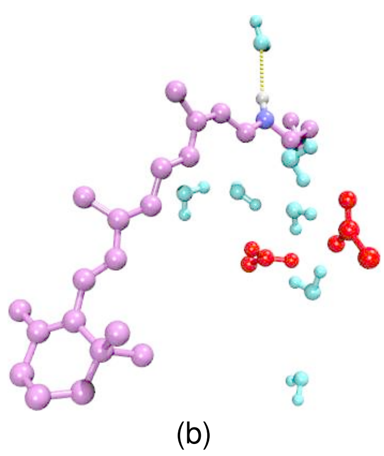

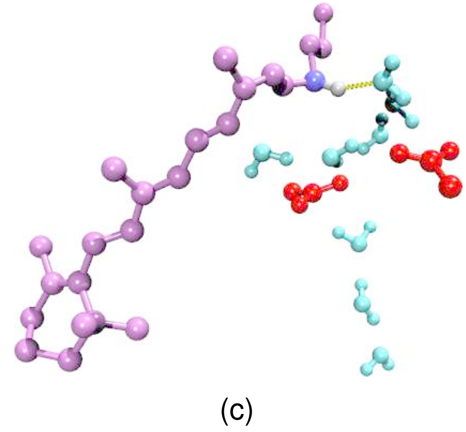

Figure 6: (a) Retinal and its binding site in bR, including residues Asp-85, Asp-212, and internal water molecules. (b) Case 1 13-*cis* photoproduct. (c) Case 2 13-*cis* photoproduct.